The Relevance of Biological Realism in a Spiking Neuron Model of Feature Detection

Robert Clewley

Spring 2000

Abstract

A one-dimensional chain of mutually inhibitory spiking neural oscillators with spike propagation delay is presented which can robustly distinguish gradients in one-dimensional inputs, for instance in an image segmentation scenario. The mechanism uses an oscillator death caused by a gradient in the input to create regions of near-uniform phase in the spike-train outputs of the network, with a clear phase difference between regions. The boundaries between these crisply defined regions correspond to the steepest gradients in the image inputs, with a sensitivity determined principally by the spike propagation delay. Thus the network can be seen as smoothing heterogeneity in input data. The mechanism relies on a biologically plausible coding of the inputs by the inter-spike intervals of a set of spike bursts, and on coding the outputs by the phase difference between the two regions created.

This work extends studies of synchronisation and oscillator death for networks of integrate-and-fire neurons with delayed mutually inhibitory connections in two ways. Firstly, it is shown that any robustness in the mechanism is possible only when shunting in the synaptic inputs and absolute refractoriness are included in the model. Secondly, analysis of both the transient and long term steady state behaviour of the network remains possible even with these added features and realistic coding. The analysis accurately predicts parameter regimes within which the network works robustly for a wide range of inputs, whilst guaranteeing the stability of the state of oscillator death for large times.

1 Introduction

Insight into the principles of neural network dynamics can be achieved by studying simple models which drastically reduce the complexity of the individual model neurons and of the network inputs and outputs. However, it is of increasing interest to understand the dynamics of extended models which include various biologically plausible features, in order to appreciate their possible relevance to mechanisms of neural computation. This work adopts the latter approach, and investigates the theoretical possibilities of modelling and analysis with biologically plausible networks, rather than modelling any particular biological system. For concreteness, the network presented in this paper will be interpreted as a model of 1D visual region segmentation (or edge detection) in a simplistic hypothetical brain. As an example, we take advantage of certain properties of a plausible signal coding in a simple network of integrate-and-fire (IF) neurons ([19]), and show how this enables a type of feature detection to be performed by a particularly simple mechanism. We also find that including other biologically plausible characteristics in the model, such as shunted synaptic inputs, spike propagation delays and refractoriness, can make a significant difference to the practicality of a computational mechanism.

The model consists of a strongly coupled one-dimensional chain of IF neurons. The computational goal of the model will be the following. That a sufficiently steep gradient ('edge') in an image will generate an output from the network which codes the position of the edge and the two regions it separates. A mechanism that acheives this should be robust, and its output stable over an appropriate length of time.

The network input will be a set of spike bursts whose inter-spike intervals (ISIs) encode the values of the image quantised over the chain. The output is designed to be a set of synchronised spike trains, of fixed ISI, in which an edge is represented by a constant phase difference between the spike trains on each side of the gradient, which is much greater than any phase drift between neurons on the same side. Coding neural signals by the ISIs of spike-trains (especially in bursts) is not common in the inputs and outputs of neuron models. Understanding the complex dynamics associated with these codes, as well as the simpler rate codes, is becoming a topic of much current interest as one seeks to understand how more realistic models act as integrated components of a larger neural system (see for example Refs. [2][14][16][24][25][27, Chapter 13]).

The mechanism used here is based on 'oscillator death', which is caused by heterogeneity in the excitatory neural inputs, and mutually inhibiting connections along the chain. Furthermore, the delayed inhibitory connections provide the approximately in-phase synchronisation between neurons on each side of the suppressed neuron, which will be referred to as the 'phasic regime', after White *et al.* [30]. Oscillator death has been dealt with in de-

tail by White *et al.* in this reference for networks of Hodgkin-Huxley neurons with synapses modelled by first order kinetics, and for IF networks of various architectures in Refs. [4][8] and [9]. The phase coding of the output could be seen as a simple form of 'temporal segmentation' of the two image regions found in other image processing networks ([17][29][20]). Several studies indicate that stimulus-induced oscillations in local neuronal assemblies (e.g. in visual cortex) are zero phase-locked over extensive cortical distances, if the stimulus contains appropriate global parameters ([10][15][22]). Other roles for phase coding in mammalian brains are discussed by Hopfield in Ref. [16].

The simplified membrane dynamics of the IF approach permits some analytical investigation of the transient dynamics underlying the mechanism. The roles of shunted synaptic inputs have also been investigated in other contexts ([1][9]).

The rest of this paper is outlined as follows. The detailed architecture of the model including the representation of inter-neuronal signals is given in §2. In §3 it is described how this architecture leads to a simple mechanism for feature detection in one-dimensional input data (after suitable coding). Numerical simulations demonstrating this mechanism and its robustness are presented in §4. The analysis of §5 focuses on the role of a particular system parameter, the propagation delay t_d, in governing the working of the mechanism. First a relationship is derived between the delay and the onset of the mechanism which is then compared to the numerically obtained relationship. Then, the linear stability of the phasic regime for long times is derived, which yields explicit formulae for two positions on the sub-threshold orbit of the suppressed oscillator via a numerically integrated continuation of a fixed point of a Poincaré return map. These predicted points are also compared to those observed in the simulations. Finally in §5 there is a brief argument to suggest how the transition from the transient dynamics during the image input burst to the long-term phasic regime might be made during successful feature detection. A discussion of the results and directions for future work form the subject of §6.

2 The model

We will assume that the class of image inputs are one-dimensional, static, and noiseless. All images will consist of two regions of approximately uniform intensity, separated by a region containing the contrast gradient. The image is discretised into an array of intensities, which are coded in the ISIs of spike-train bursts fed to the network's inputs. We model a 'patch' of N IF neurons within the network, where N is assumed small enough for the patch to contain only one contrast gradient between two regions.

The patch consists of a chain of neurons modelled by IF dynamics with additional biologically-realistic features. The IF formalism ignores the detailed

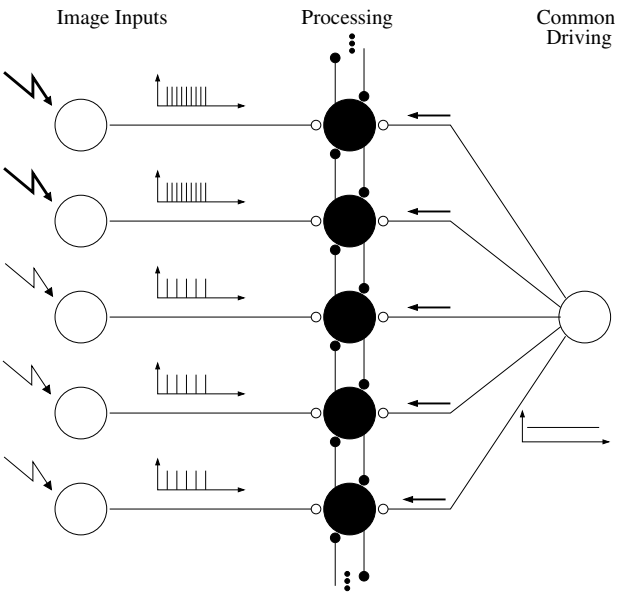

Figure 1: **The network architecture for five integrate-and-fire neurons within a chain.** Connections terminating in open circles represent excitatory synapses; those terminating in solid circles represent inhibitory synapses. Thick 'lightning' arrows represent stronger intensities in the image than the thin arrows.

form of individual spikes ([19]). The benefit is that detailed analytical investigations of the dynamics of simple IF networks are possible (e.g. [4][13]), as the linearity of a sub-threshold IF membrane equation enables a reduction to an implicit firing-time map. Thus the IF model is an ideal basis for analytically investigating the role of biologically plausible features in network-based computations. At the level of individual neurons, the features included here are fixed spike propagation delay, semi-realistic post-synaptic currents, and absolute refractoriness. At the network level, the use of the IF model simplifies the study of computational mechanisms because they are based on the 'coding' of inputs and outputs by ISIs rather than by firing rates.

The simple architecture of the chain of N identical neurons is depicted in Figure 1. The i^{th} neuron is assumed to have a membrane potential denoted $U_i(t)$, for $t > 0$. When $U_i(t)$ reaches a fixed threshold θ then $U_i(t)$ is reset instantaneously to a resting potential (chosen to be zero in suitable units). This reset represents the firing of a spike of electrochemical activity along the neuron's axon. Let $T_{U_i}^n$ denote the time at which neuron i fires on the n^{th} occasion since $t = 0$, written as

$$T_{U_i}^n = \inf\left\{t \mid U_i(t) \geq \theta;\, t > T_{U_i}^{n-1} + t_R\right\}, \tag{2.1}$$

where t_R denotes a period of absolute refractivity, during which the neuron is not allowed to fire. The evolution of the membrane potentials is given by a set of linear ordinary differential equations

$$\frac{dU_i(t)}{dt} = -\tau U_i(t) + \sum_{j \neq i} W_{ij} g_{ij}(t) \left[S_{ij} - U_i(t)\right] + g_i(t) \left[S_E - U_i(t)\right] + I, \quad (2.2)$$

describing the excitable dynamics for $0 < U_i(t) < \theta$, and the discontinuous reset conditions

$$\lim_{\varepsilon \to 0_+} U_i(T^n_{U_i} - \varepsilon) = \theta, \quad \lim_{\varepsilon \to 0_+} U_i(T^n_{U_i} + \varepsilon) = 0. \quad (2.3)$$

Here, τ is a membrane leakage time constant, and W_{ij} is a matrix describing the chain's connectivity. The term $g_{ij}(t)$ represents the post-synaptic response current from synapse (ij), and S_{ij} is the so-called membrane reversal potential. Similarly, $g_i(t)$ is the synaptic response to the input from the i^{th} point of the discretised image, which is shunted according to the constant reversal potential S_E, which is positive for an excitatory synapse and negative for an inhibitory one. A constant drive $I > \tau\theta$ is applied to each neuron so that in the absence of interactions it acts as a regular oscillator by firing spikes with a constant period $\frac{1}{\tau} \ln \left[I / \left(I - \tau\theta\right)\right] + t_R$. The matrix W_{ij} describes nearest-neighbour coupling defined by

$$W_{ij} = \delta_{j,i+1} + \delta_{j,i-1}, \quad (2.4)$$

where δ is the Kronecker delta function. Throughout this paper the initial conditions (when $t = 0$) for U_i will be assumed to be zero for all i.

The following simple interpretation of the inter-neuronal communication process is assumed. A spike fired by neuron j along its axon arrives at a neighbouring neuron i via the synapse (ij), and elicits a post-synaptic response current $g_{ij}(t)$. This response current excites the somatic membrane potential $U_i(t)$ by an $\mathcal{O}(1)$ amount according to the i^{th} equation of (2.2). Despite the dynamic properties of biological synapses (e.g. [21]), and adaptive properties related to learning, the synaptic response $g_{ij}(t)$ elicited by a spike will be assumed to be independent of recent synaptic activity, and defined by

$$g_{ij}(t + t_d) = \sigma_{ij} \sum_{n \geq 1} h\left(t - T^n_{U_j}\right). \quad (2.5)$$

Here, the $\sigma_{ij} > 0$ represent coupling strengths, assumed identically equal to a constant σ, $h\left(\cdot\right)$ is a post-synaptic response function, and the delay time t_d incorporates both the axonal and dendritic tree spike propagation times. In this paper we need only assume five general conditions on the function $h(\cdot)$:

$$\left.\begin{array}{lcl} h(s) & \geq & 0 \quad \text{for all} \quad s, \\ h(s) & = & 0 \quad \text{for all} \quad s \leq 0, \\ \int h(s)\, ds & = & 1, \\ \lim_{s\to\infty} h(s) & = & 0, \\ q_T(s) & = & \lim_{k\to\infty} \sum_{j=1}^{k} h(s+jT) < \infty, \quad \text{for all} \quad s \geq 0, \end{array}\right\} \tag{2.6}$$

where T is a constant time period. These conditions reflect the fact that the following analysis is not specific to a particular synaptic response model, although they are met by the standard alpha-function models used in the literature such as

$$h(s) = \alpha^2 s e^{-\alpha s} \Theta(s), \tag{2.7}$$

where $\Theta(\cdot)$ is the Heaviside function (e.g. see Ref. [18]). The final condition in (2.6) ensures the convergence of the geometric progression to a finite limit for each finite s and T. Typically $h(\cdot)$ and T are given in closed form, in which case $q_T(s)$ will also be in closed form.

Since we are modelling a finite chain, complications can arise in its numerical simulation due to cut-off effects at the two ends. We use a 'mirror' boundary condition to lessen these effects, whereby the last two neurons at each end have identical image inputs, so that their dynamics are identical. The resulting symmetry allows the mutually inhibitory inputs 'missing' from the last neuron to be implemented by doubling that neuron's coupling strengths σ.

For simplicity the coding of the image input burst to neuron i will be assumed to have a fixed duration t_{burst}, a constant ISI λ_i, and a fixed amplitude of 1 (i.e., it has a square-wave envelope). We define λ_i to be inversely proportional to the i^{th} image pixel intensity. From this, the firing times within the i^{th} burst are denoted $T^n_{im_i}$, so that $T^n_{im_i} = (n-1)\lambda_i$ is the ISI, for n between 1 and n_i (with $T^1_{im_i} > 0$ and $T^{n_i}_{im_i} \leq t_{burst}$). We avoid considering the small spike propagation delay from the source of this spike burst by absorbing the delays into the firing times $T^n_{im_i}$, and ensuring that the firing times are all greater than zero. Thus the post-synaptic currents due to this input are given by

$$g_i(t) = \sigma_{im} \sum_{n\geq 1} h\left(t - T^n_{im_i}\right), \tag{2.8}$$

where $\sigma_{im} > 0$ is a synaptic coupling strength (identical along the chain), and the synaptic response function $h(\cdot)$ satisfies (2.6).

3 The mechanism

The typical behaviour of five neurons near a simple image contrast is shown in Figure 2. The reversal potential $S_E > 0$ ensures that the image input synapses are excitatory. As White *et al.* have discussed in detail in Ref. [30] in the context of heterogeneity, the asymmetry in excitation near the site of the contrast for $t < t_{burst}$ means that the neurons in one region fire their first spike before those in the other region. For suitable choices of free parameters the neuron at the boundary of the faster spiking region can cause the suppression of its neighbour in the slower spiking region, as depicted in Figure 3. Here we will view the oscillator death as a bifurcation in the solutions of the ODE system (2.2).

A suppressed neuron forms a 'boundary' between the other neurons in the chain, and is used to represent the successful segmentation of an image into two regions. The parts of the chain above and below the boundary will be called the 'upper region' and 'lower region' respectively. The image burst (for $t < t_{burst}$) sets up a phase difference between the two regions, while within each region an almost constant phase relationship is maintained, which remains stable for some time after the formation of the boundary. This phasic regime is a form of output that can code information for further levels of processing in a biologically plausible fashion. The fact that connectivity is strictly nearest-neighbour means that there is no interaction between the upper and lower regions whilst the boundary exists. The apparent stability of the phasic regime in each region of the chain is partly due to the delayed inhibitory coupling in the chain, and the choice of membrane equations (2.2). The reversal potentials for connections within the chain are identically constant so that $S_{ij} \equiv S_I \leq 0$, providing mutual inhibition along the chain. The synaptic response is a positive function, which in the context of an IF equation means the membrane dynamics can be categorised as Type I, in the sense of Ref. [11]. One implication of this is that in-phase synchronisation is a stable solution for the neurons in the absence of image input ([28]). Furthermore, for mild heterogeneity in the system, near-synchronisation is still stable for these equations (e.g. see [23][30]). Here, for instance, an image may contain small-scale fluctuations away from the position of principal contrast, and the mechanism remains robust.

If the asymmetry in the input is insufficient to cause the neuron's suppression before t_{burst} then suppression will not occur, since the inputs return to a symmetric state for $t > t_{burst}$. Numerical simulations have revealed that for some parameter regimes the neuron at the boundary may fire one or more transient spikes before being suppressed and entering the phasic regime, but the current investigation focuses on the case of zero transient spikes. We will therefore interpret successful 'detection' to mean that oscillator death occurs near the site of greatest contrast in the image for $t < t_{burst}$, and the system settles to the long-term phasic regime centred on the suppressed oscillator.

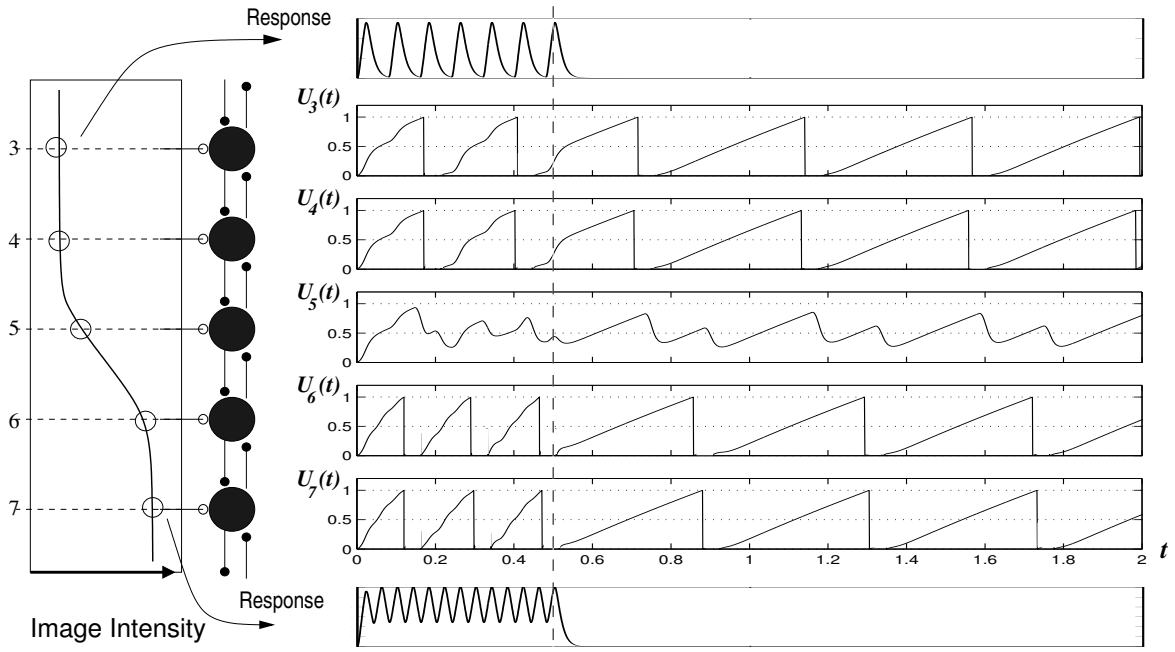

Figure 2: **Typical network activity.** A sample of typical network activity on successful detection of an edge, or equivalently, segmentation of two intensity regions. The dashed line across the time plots marks the end of the image input spike burst at $t = t_{burst}$. The output was created by direct simulation of (2.1)-(2.8) with the parameter values (4.2) with $\lambda_{lo} = 0.08$, $\lambda_{hi} = 0.04$, $w = 0.05$, $\sigma = 1.275$, and $t_d = 0.025$.

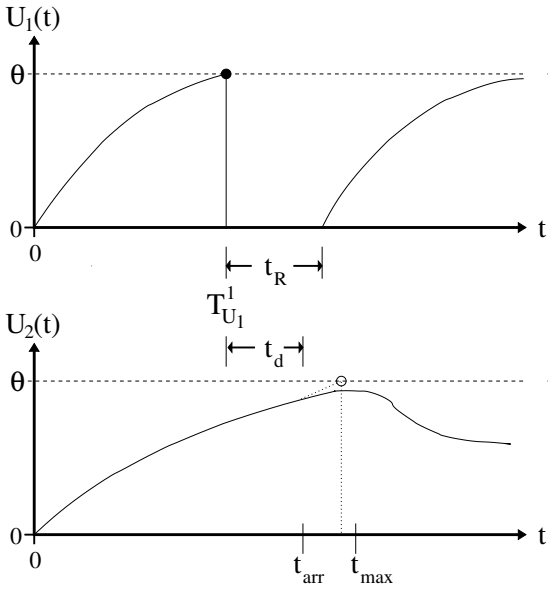

Figure 3: **A schematic diagram of the onset of oscillator death.** The first spike of neuron 1 occurs at $T^1_{U_1}$, and arrives at its neighbour, neuron 2, after a propagation delay t_d, at a time t_{arr}. As a result of the inhibition this spike causes in neuron 2, $U_2(t)$ fails to reach threshold and instead has a maximum at time t_{max}. The dotted line indicates the time at which neuron 2 would have fired in the absence of the inhibition.

The shunting feature, i.e. the terms $[S_{ij} - U_i(t)]$ and $[S_E - U_i(t)]$ in (2.2), effectively scales the effect that a synaptic response has on a membrane potential $U_i(t)$ in proportion to how close $U_i(t)$ is to the reversal potential. This property suggests a reason for the striking robustness of the segmentation mechanism seen in the simulation results which follow, since shunting plays its most significant role in the inhibitory interactions within the chain. Removing the shunting feature from the model was found to cause further oscillator deaths in positions away from the image contrast, despite the known stabilising effect that delayed inhibitory coupling has for small phase variations between neurons. Shunting can thus be seen as providing soft tolerance to phase drift in the context of inhibitory connections. The inclusion of an absolute refractory period t_R improves the situation further, in a fashion akin to an extreme form of shunting. It provides a strong tolerance window in which the effect of an input arriving near to the neuron's own firing time is almost completely eliminated, with only its tail contributing an amount after t_R (which itself will be lessened by shunting). From simulations of the model without the inclusion of an absolute refractory period, only a small range of parameters and image inputs caused segmentation with zero transient spikes in the suppressed neuron, and many additional oscillator deaths occurred away from the contrast, disrupting the mechanism.

It is important to note that the choice of the axonal and dendritic delay constant t_d has a highly intuitive effect on the image processing mechanism: it works as a control of contrast-versus-noise sensitivity, determining a time-window within which arriving spikes will be treated as belonging to another intensity region rather than an in-region variation in firing times. Given its role in the segmentation mechanism, t_d is used as a bifurcation parameter in the following investigation of successful segmentation regimes, although other system parameters could equally well have been used.

4 Numerical Simulations

We shall now present the results of numerical simulations designed to investigate how the segmentation mechanism depends on various free parameters, particularly t_d. The simulations were carried out within MATLAB [26].

The following simple model of a noiseless image contrast was used for the numerics. The ISIs λ_i of the incoming spikes in the image input burst to the i^{th} neuron were determined by discrete sampling of a tanh function, expressed here in the discrete spatial variable $x = i - \llcorner N/2 \lrcorner$ (where $\llcorner \cdot \lrcorner$ denotes the integer part of),

$$\lambda_i = \lambda_{hi} + \frac{1}{2}\left(\lambda_{lo} - \lambda_{hi}\right)\left[1 + \tanh\left(\frac{x-a}{w}\right)\right]. \tag{4.1}$$

The parameters in this formula control the features of the 1D image: λ_{lo} and

λ_{hi} are the lower and upper asymptotes of the image intensities (proportional to the inverse ISIs) at either side of the edge, a is the degree of asymmetry about the centre of the gradient, and w governs the width of the gradient. By choosing $w < 0.1$ it was found that the discretisation of an image was piecewise-constant to 4 decimal places. By approximating a step function in this way we obtained a simple test image having a perfectly sharp contrast.

The following table gives the range of parameter values used in this paper.

$$\begin{array}{lll} \tau = 0.5 & t_{burst} = 0.5 & \lambda_i \in [0.04, 0.15] \\ \sigma_{im} = 0.34 & S_E = 1.3 & w \in [0.05, 1.6] \\ \sigma \in [0.15, 1.5] & S_I = 0.0 & a = 0.5 \\ t_d \in [0.005, 0.06] & \theta = 1 & N = 9 \\ t_R = 0.043 & I = 3.0 & \end{array} \tag{4.2}$$

The form of $h(\cdot)$ used here closely resembles the simple alpha function (2.7) and satisfies the general conditions (2.6). A full definition and associated computational details is given in the Appendix.

4.1 Robustness on varying the coupling strength

Figure 4 shows the effect of varying the coupling strength σ. The results in the graph correspond to data for three perfectly sharp image contrasts. For each σ the maximum value of t_d was found such that the onset of oscillator death occurred near the position of the contrast gradient with zero transient spikes. Note the shallowness of the incline for each curve of increasing σ, signifying the reliability of the mechanism for a wide range of σ values. Figure 5 shows maxima of t_d for the occurrence of zero, one and two transient spikes together, for image 2 in the previous figure. (The value $t_{burst} = 0.5$ used dictates a maximum of two transient spikes before a possible oscillator death.) These results show that for some images successful feature detection remains possible for longer delays. It was also found that sufficiently large values of σ (e.g. greater than 0.7) ensured that the phasic regime was always entered after the suppression occurred. Similar results obtained for image 3 of Figure 4, which has a lower average intensity, show that the separation between the curves which define the regimes with zero, one and two transient spikes was significantly smaller, as was the absolute range of t_d values for zero transient spikes.

In both figures, data points are missing for sufficiently low values of σ, where the mechanism breaks down entirely, typically with no sustained oscillator death. This is due to disruption by other inhibitory spikes, the weakness of inter-neuronal coupling (i.e., small σ values) or the weakness of the image input driving. For some larger values of σ disruption is still observed after oscillator death, so that the phasic regime may not be entered. Due to the

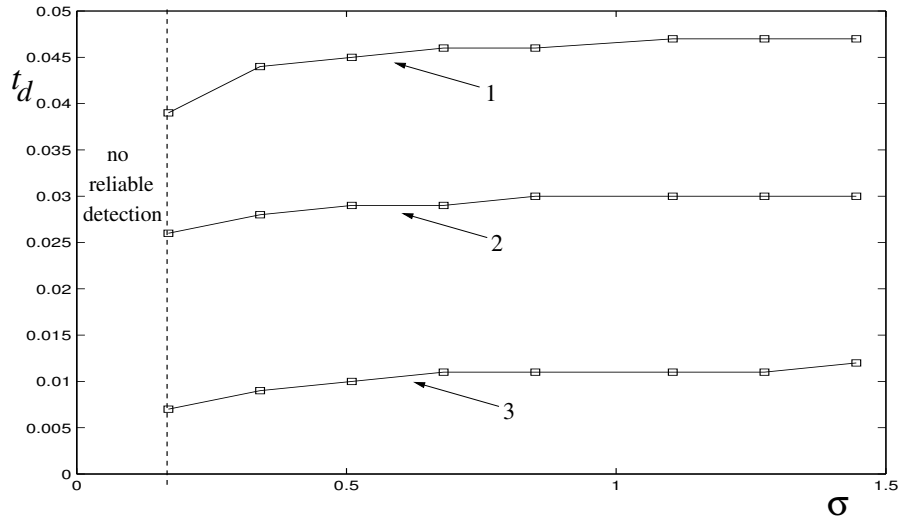

Figure 4: **Robustness on varying connection strength.** For a given image, at each fixed value of σ the maximum value of t_d was found such that oscillator death occurred with zero transient spikes. Curves for three images are shown: (1) $\lambda_{hi} = 0.04$, $\lambda_{lo} = 0.08$; (2) $\lambda_{hi} = 0.06$, $\lambda_{lo} = 0.10$; (3) $\lambda_{hi} = 0.08$, $\lambda_{lo} = 0.12$. All other parameters are as in (4.2) with $w = 0.05$. The dashed line marks the approximate lower limit of σ for which detection is possible.

complications arising from multiple interactions in these cases, the precise lower bound on σ for successful transition to the phasic regime are not easily determined.

Although smaller values of t_d permit a larger range of gradients to be detected in the inputs, in several simulation runs values under 0.01 were found to cause over-sensitivity to variations in the firing times of neighbouring neurons, especially if heterogeneity in the inputs or the neurons was present. This led to unwanted oscillator deaths in other sites of the chain, disrupting the phasic regime. The disruption was either *(a)* that a single additional neuron in one region becomes suppressed, whilst the phase difference across the remaining neurons in the region remains small, or that *(b)* the original suppressed neuron re-fired, so that within a small multiple of the phase-locked firing period the disruption propagated along the chain, destroying all the region and phase information in the output.

4.2 Sensitivity of the network

Next, Figure 6 shows the results of taking a range of simple images with varying contrast depth, generated using (4.1) in the following way. By choosing $w = 0.05$ so as to make the image almost a step function, and relating the two asymptotes of the image by

$$\lambda_{lo} = \lambda_{hi} + c, \tag{4.3}$$

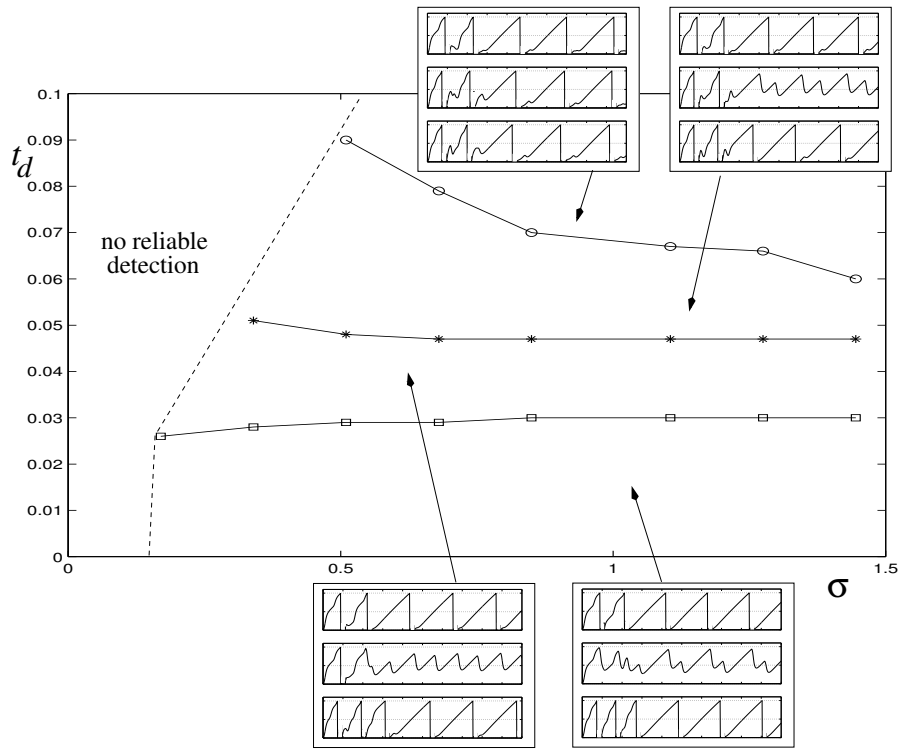

Figure 5: **Robustness on varying connection strength (additional transient spikes)** for $\lambda_{hi} = 0.06$, $\lambda_{lo} = 0.10$. At each fixed value of σ the maximum value of t_d was found such that oscillator death occurred with zero transient spikes (squares), one transient spike (stars) and two transient spikes (circles). All other parameters are as in (4.2) with $w = 0.05$. The insets show time histories for the three neurons straddling the contrast site.

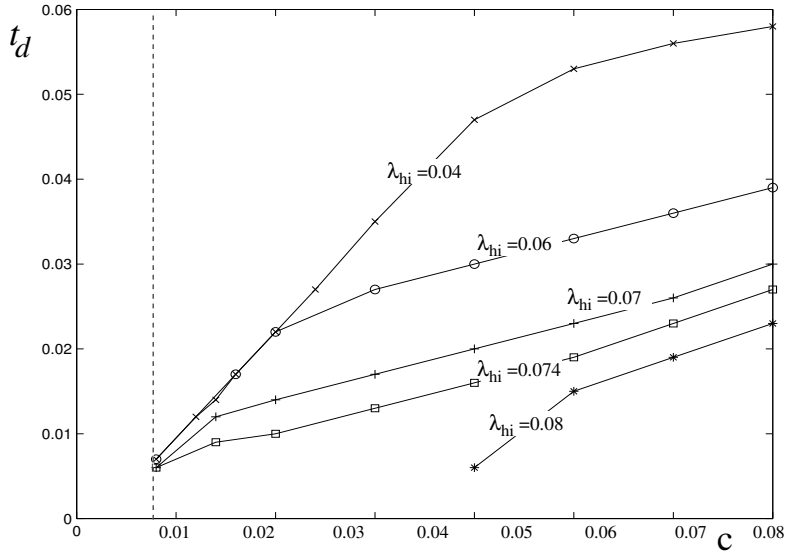

Figure 6: **Sensitivity of the detector.** For each value of λ_{hi} shown, and for each fixed contrast c, the critical value of t_d was found such that below it, oscillator death occurs with zero transient spikes, and above it oscillator death occurs with one transient spike. All other parameters are as in (4.2) with $w = 0.05$, $\sigma = 1.275$ and λ_{lo} given by the relationship (4.3).

a measure of the contrast depth c and reference intensity λ_{hi} were used as independent variables. For a given λ_{hi}, a range of values were taken for c, for which the highest value of t_d was found such that *(a)* an oscillator death occurred with zero transient spikes, and *(b)* the suppressed state remained sub-threshold for $t \leq t_{burst}$. Data points were not found for contrasts so small that $t_d < 0.005$ was required, since it was found that such small values of t_d caused over-sensitivity in the network that led to extra oscillator deaths, disrupting the mechanism. Notice that the minimum detectable c increases dramatically past a certain value of λ_{hi}. This is due to the spiking nature of the image inputs. For small increases in the input ISIs, their combined effect with the fixed background driving input I will cause periods of steady increase in the time-to-first-spike of a neuron, until the ISI is large enough that one spike no longer contributes before the drive I causes a firing, thus the time-to-first-spike will increase sharply. Thus the drive I increasingly determines the next firing time of the neuron as the image inputs with small λ_i contribute less. This also explains why curves for higher values of λ_{hi} flatten out strongly after smaller increases in c: the effect on the dynamics over the short time t_{burst} of the input with larger ISI (λ_{lo}) is less in comparison to the drive I.

Figure 7 presents a similar set of test results, by varying the gradient width w, and using $\sigma = 1.275$, $\lambda_{lo} = 0.08$ and $\lambda_{hi} = 0.04$. A starting point was taken to be a parameter regime in which a contrast of width $w < 0.1$ could be successfully processed with zero transient spikes before suppression,

for some maximum t_d. Then w was increased and the new maximum t_d found such that oscillator death occurred with zero transient spikes. The results demonstrate that the network is able to cope with relatively blurred edges. Since the mechanism of oscillator death works on the steepness of local gradients in the image inputs, greater widths w (e.g. $w > 1.0$) of the overall image gradient mean that more than one neuron may become suppressed, typically within one or two positions of the original position. The network may still make a transition to a stable phasic regime in these circumstances, with three or more regions of near-uniform phase set up for $t > t_{burst}$, although it was found that the interplay of the several additional inter-neuronal spikes now involved during the burst period made prediction of any particular outcome difficult.

The network's robustness on introducing a low level of heterogeneity to the inputs was also investigated. This entailed perturbing each of the ISIs λ_i (derived from a particular image) by an amount randomly sampled from a standard Gaussian distribution, whose variance was used as a controlling parameter. Several runs were then performed and the onset of oscillator death after zero transient spikes was found each time by varying t_d in a similar fashion to the tests previously described. This procedure was repeated for different values of σ and the maximum values of t_d found were compared to those shown in Figure 4. The strictly nearest-neighbour nature of the processing mechanism suggests that moderate differences in two neighbouring image input ISIs would be processed as a small contrast in the image. In particular, this means that if the delay t_d was tuned away from sensitivity to these small variations then the network would tolerate the heterogeneity, just as it would not undergo an oscillator death to a genuine image contrast of that size. Thus it was found that for perturbations significantly smaller than the size of the image contrast, and with an appropriate value of t_d to detect the contrast, the network would respond almost identically as it would in the absence of heterogeneity (data not shown). For the same reason, the network was tolerant to the presence of mild heterogeneity in the ISIs of the image input spike bursts. An extensive study of heterogeneity and time dependent noise in this model is a topic for future work, but is analysed in some detail for a similar network in Refs. [8][30].

Having demonstrated a relationship between the delay constant t_d and the robustness and sensitivity of the segmentation mechanism, we shall next proceed with an analysis to explain some of these numerical results.

5 Analysis

By a renumbering of the positions in the chain, let $U_1(t)$ and $U_2(t)$ denote the membrane potentials of two neurons lying either side of the largest gradient in the image, which for simplicity we shall assume to be a single step contrast.

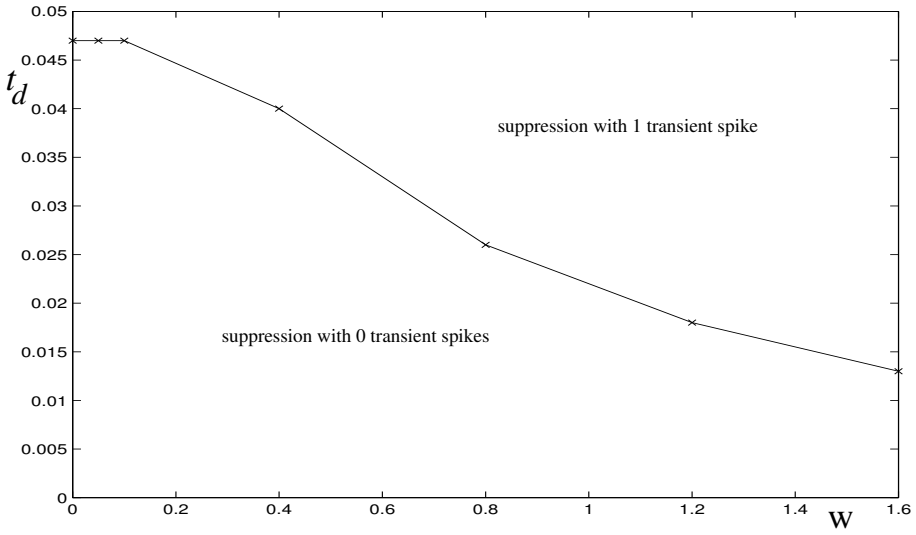

Figure 7: **Effect of varying width on robustness.** For a fixed contrast the width w is varied and critical values of t_d found that delimit regimes in which oscillator death with zero and one transient spikes occur. For this data, $\sigma = 1.275$ and $\lambda_{hi} = 0.04$, $\lambda_{lo} = 0.08$, otherwise all parameters are as in (4.2).

Also, neuron 1 will denote the neuron forced more strongly from the image input. We will investigate the transient, the long-term, and transitional aspects of the segmentation mechanism thus:

(I) We first seek bounds on t_d in order that the onset of oscillator death in neuron 2 occurs after zero transient spikes.

(II) We next seek stability conditions on the persistence of neuron 2's suppressed state in an idealised, long-term approximation to the system, and show that $U_2(t)$ tends to a periodic sub-threshold orbit.

(III) We argue how it may be possible to link the conditions made in (I) for the transient dynamics to the conditions for long-term stability of the phasic regime in (II). This is relevant because following the decay of the response to the spike that suppressed neuron 2, $U_2(t)$ will increase once more, and the mechanism must prevent neuron 2 from firing again in order to make the transition to the phasic regime.

5.1 The onset of oscillator death

The simulations demonstrated that detectable contrasts can be generated with only a small corresponding variation in the spike train ISIs λ_i of the image inputs. For the present purposes, it will therefore be convenient to assume that the difference in ISI between the neurons either side of an edge is small enough so that neuron 1 does not fire multiply in the time that neuron 2 takes to fire once (in the absence of all inhibitory interactions). Thus only one input from neuron 1 must be considered to study the onset of oscillator death with no transient spikes from neuron 2. We may therefore

focus on the behaviour of the reduced system

$$\frac{dU_1(t)}{dt} = -\tau U_1(t) + \sigma_{im} \sum_{n\geq 1} h\left(t - T^n_{im_1}\right)\left[S_E - U_1(t)\right] + I \qquad (5.1)$$

$$\frac{dU_2(t)}{dt} = -\tau U_2(t) + \sigma_{im} \sum_{n\geq 1} h\left(t - T^n_{im_2}\right)\left[S_E - U_2(t)\right] + I$$
$$+\sigma h\left(t - T^1_{U_1} - t_d\right)\left[S_I - U_2(t)\right], \qquad (5.2)$$

for $0 \leq t < T^1_{U_1}$, with zero initial conditions. The pre-spiking solution for $U_1(t)$ can now be used to give $T^1_{U_1}$ implicitly, since by definition $U_1(T^1_{U_1}) = \theta$:

$$\theta = P_1\left(-T^1_{U_1}\right) \int_0^{T^1_{U_1}} \left\{ I + S_E \sigma_{im} \sum_{n\geq 1} h\left(u - T^n_{im_1}\right) \right\} P_1(u)\, du, \qquad (5.3)$$

where

$$P_1(s) = \exp\left(\tau s + \sigma_{im} H_1(s)\right), \qquad (5.4)$$

and

$$H_1(s) = \sum_{n\geq 1} \int_0^s h\left(v - T^n_{im_1}\right)\, dv. \qquad (5.5)$$

Unequal image inputs are the only source of asymmetry in the mechanism, and so must be present long enough to allow the possibility of oscillator death. Hence we must ensure throughout that the system parameters are such that t_{burst} is greater than the times $T^1_{U_1}$, t_{arr}, and t_{max}, where t_{arr} is the arrival time of the spike generated at $T^1_{U_1}$, and t_{max} is the time of the subsequent turning point in $U_2(t)$ (see Figure 3). By assumption, neuron 1 fires before neuron 2, and so for this case $t_{arr} < T^1_{U_2}$, i.e. the delay t_d is sufficiently small that neuron 2 has not fired when the spike from neuron 1 arrives.

We wish to ensure that $U_2(t)$ reaches a local maximum below the threshold and then decreases as a result of the single inhibitory pulse received from neuron 1, for $t < t_{burst}$. By integrating (5.2) the pre-spiking solution for $U_2(t)$ under the influence of neuron 1's first spike we find a limiting condition on t_d, under which neuron 2 undergoes a subsequent turning point at $t = t_{max} > t_{arr}$ just under the threshold. The first turning point of $U_2(t)$ is a local maximum because the interaction terms are non-positive. By formally requiring that the maximum occurs at threshold, the required condition on t_d comes from numerical solution of the following two implicit simultaneous equations in the two unknowns t_{max} and t_{arr}.

$$\theta = P_2(-t_{max}) \int_0^{t_{max}} \{I + \sigma_{im} S_E \sum_{n\geq 1} h\left(u - T^n_{im_2}\right) + \sigma S_I h\left(u - t_{arr}\right)\} P_2(u)\, du, \quad (5.6)$$

$$h\left(t_{max} - t_{arr}\right) = \frac{I + \sigma_{im}\left(S_E - \theta\right) \sum_{n\geq 1} h\left(t_{max} - T^n_{im_2}\right) - \tau\theta}{\sigma\left(\theta - S_I\right)}, \quad (5.7)$$

where

$$P_2(s) = \exp\left(\tau s + \sigma_{im} H_2\left(s\right) + \sigma \int_0^s h\left(v - t_{arr}\right)\, dv\right), \quad (5.8)$$

and

$$H_2\left(s\right) = \sum_{n\geq 1} \int_0^s h\left(v - T^n_{im_2}\right)\, dv. \quad (5.9)$$

We therefore have an implicit analytical expression for the upper bifurcation value of the parameter $t_d = t_{arr} - T^1_{U_1}$, provided that $h(\cdot)$ can attain the critical value given by (5.7). This is possible only *(a)* if the right hand side of (5.7) is in the interval $[0, 1]$, the range of $h(\cdot)$; and *(b)* if the inverse rise time (given by α^{-1} for a simple alpha function such as (2.7)) of $h(\cdot)$ is sufficiently high so that it is possible to reach the required value in time. Thus for slow synapses or inhibitory spikes generated very late, even instantaneous propagation of the spike ($t_d = 0$) may not be enough to prevent neuron 2 from reaching threshold. However, so long as these two conditions are met, then there is a non-zero value of t_d that solves (5.6, 5.7). Clearly, any inhibitory spike from the more strongly driven neighbour propagating faster than the upper bifurcation value for t_d whilst $U_2(t) < \theta$ will also allow the response $h(\cdot)$ to reach the critical value at some shorter time than the critical t_{max}, so that the maximum $U_2(t_{max})$ will also be sub-threshold. Thus there is no *lower* bifurcation point for t_d under which oscillator death does not occur, although there is a *practical* lower limit on t_d. Low t_d values can cause unwanted additional oscillator deaths in positions away from the principal contrast (usually for $t > t_{burst}$) because the mechanism is then over-sensitive to intensity variation across the image.

Formula (5.7) gives the critical value that the inhibitory response $h\left(t_{max} - t_{arr}\right)$ must reach at time $t = t_{max}$ to cause a maximum at $U_2\left(t_{max}\right) = \theta$, and shows that this critical value increases with the strength of the excitatory input, i.e. with an increasing number of image input spikes arriving before t_{max}. We can derive a corresponding condition to (5.7) for a simpler model in which shunting is neglected (and instead the signs of σ_{im} and σ determine excitatory or inhibitory connections) thus:

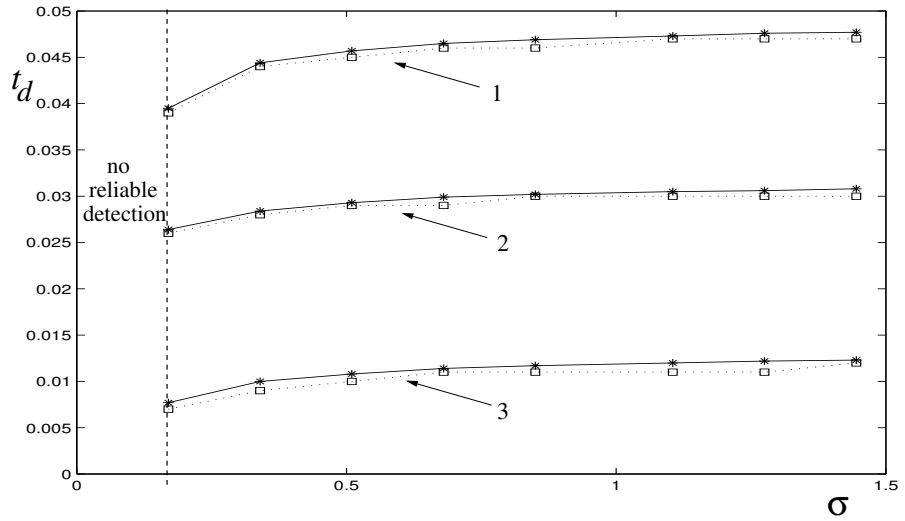

Figure 8: **Numerically computed solutions of (5.6) and (5.7), determining the onset of oscillator death.** For a given image, at each fixed value of σ the critical value of t_d was found that separates the regimes of oscillator death with zero and one transient spikes. The calculation of these critical values from equations (5.6) and (5.7) are shown as dotted lines, whilst observed data from simulations is shown as solid lines. Curves for three images are shown: (1) $\lambda_{hi} = 0.04$, $\lambda_{lo} = 0.08$; (2) $\lambda_{hi} = 0.06$, $\lambda_{lo} = 0.10$; (3) $\lambda_{hi} = 0.08$, $\lambda_{lo} = 0.12$. All other parameters are as in (4.2) with $w = 0.05$. The dashed line marks the approximate lower limit of σ for which detection is possible.

$$h\left(t_{max} - t_{arr}\right) = \frac{I + \sigma_{im} \sum_{n \geq 1} h\left(t_{max} - T^n_{im_2}\right) - \tau\theta}{|\sigma|}, \qquad (5.10)$$

where $\sigma_{im} > 0$ and $\sigma < 0$. From (5.10) it is possible to see how including the shunting terms in the present model improves robustness (particularly for the inhibitory inputs) for standard choices of reversal potentials S_E and S_I. For simplicity, suppose $\theta = 1$. Typically, we then choose $S_E - \theta < 1$. By inspection of the two formulae for the critical values, the inclusion of shunting on the excitatory image inputs decreases the critical value that must be reached. Furthermore, $S_I \leq 0$ implies that $\theta - S_I \geq 1$, which by inspection of the denominators in the two formulae shows that again the critical value is decreased by including shunting terms.

Observe that we have reduced the location of the bifurcation value of t_d defining the onset of oscillator death to the solution of two implicit equations, (5.6) and (5.7). This 'semi-analytical' form of the solution highlights the role of each term in determining the bifurcation value, and is also easy to calculate numerically, for instance using the MAPLE package [7]. Such a numerical calculation of the solutions is demonstrated in Figure 8, and it is unsurprising that these calculations yield results so close to the bifurcation values observed from direct numerical integration of the system.

5.2 A long-term periodic solution

A suppressed neuron, having a membrane potential which we will denote $U(t)$, receives two inhibitory spike train inputs from its neighbours. From simulations it is seen that in most cases the suppressed state appears to be periodic and in general remains stable long after the image input burst if sufficiently strong and frequent inhibitory spikes arrive. We will search for a sub-threshold periodic solution for $U(t)$ as $t \to \infty$, and investigate its stability. To do this, we shall make the assumption that the phases of the oscillators in each of the upper and lower regions are identical, so that the two inhibitory inputs to the suppressed neuron are T-periodic in time, and differ in phase by an amount Δ. These inputs can therefore be characterised by the arrival times $t = 0 \mod T$ and $t = \Delta \mod T$, after shifting the time axis to an arbitrary spike arrival time at the suppressed neuron (and provided $t \gg t_{burst}$). First, we write the membrane equation for $U(t)$ (in rescaled time) in a convenient form:

$$\begin{aligned} \frac{dU(t)}{dt} &= -\left[\tau + \sigma\bar{h}(t) + \sigma\bar{q}_T(t)\right] U(t) \\ &\quad + I + \sigma S_I\left[\bar{h}(t) + \bar{q}_T(t)\right], \end{aligned} \tag{5.11}$$

for some initial condition $U(0)$, and where

$$\bar{h}(s) = h(s) + h([s + T - \Delta] \mod T), \tag{5.12}$$

$$\bar{q}_T(s) = q_T(s) + q_T([s + T - \Delta] \mod T). \tag{5.13}$$

Integrating this over a period T between two spike arrival times, we only need consider the inhibitory response to one new spike from each neighbour and to the (monotonically decaying) background input $\bar{q}_T(s)$. Thus

$$U(T) = \beta\left[U(0) + \gamma\right] \tag{5.14}$$

defines a map, where

$$\beta = P(T), \tag{5.15}$$

$$\gamma = \int_0^T \left\{I + \sigma S_I\left(\bar{h}(u) + \bar{q}_T(u)\right)\right\} P(u)\, du \tag{5.16}$$

and

$$P(u) = \exp\left(\tau u + \sigma H(u) + \sigma Q_T(u)\right), \tag{5.17}$$

$$H(u) = \int_0^u \bar{h}(s)\, ds, \tag{5.18}$$

$$Q_T(u) = \int_0^u \bar{q}_T(s)\, ds, \tag{5.19}$$

with $H(u) > 0$, $Q_T(u) > 0$, which implies, crucially, that $\beta \in (0, 1)$.

U_Δ is a T-periodic solution of (5.14) if $U(0) = U(T) = U_\Delta$, so that U_Δ must satisfy

$$U_\Delta = \frac{\beta\gamma}{1-\beta}. \tag{5.20}$$

This represents one of two values reached by $U(t)$ just before attaining a maximum, since there are two inhibitory spikes arriving each period. By symmetry, the other is found by repeating the above calculation with $T - \Delta$ substituted for Δ, thus finding $U_{T-\Delta}$. This is necessary, since it remains to check that the candidate solution for (5.11) remains sub-threshold, for which the greater of the two solutions to the map is required. Taking U_Δ to be the greater, without loss of generality, the sub-threshold condition is checked by integrating (5.11) forward from initial condition U_Δ to check that the maximum reached is below θ. Analytically, this is achieved using calculations similar to those used to study the onset of oscillator death.

The stability of the periodic solution is simple to determine since the map (5.14) is affine, and $\beta \in (0, 1)$. Hence the solution U_Δ, and thus $U(t)$, is asymptotically stable, with a basin of attraction constituting the whole range of $U(t)$, namely $[0, \theta]$.

From these calculations, solutions to the map for three different images were compared to data obtained by simulation, as shown in Table 1. The parameter values used are given in the table where they were not already fixed in (4.2).

In each simulation, the differences between several spike arrival times from one neighbour were used to estimate T, and the final two times of arrival from that neuron, t_1 and t_2, were used to find the *observed* $U(t_{1,2})$, which are approximate fixed points of the periodic return map. The convergence of $U(t)$ to the predicted fixed point U_Δ is clearly rapid despite the times $t_{1,2}$ only being small multiples of the estimated T, and despite the potential source of disturbance from the non-neighbouring oscillators in each region. (Recall that although the image intensity profile was approximately a step function, oscillators neighbouring the suppressed neuron receive half the amount of in-chain inhibition compared to the other oscillators, which can cause phase drifts.) This rapid convergence is confirmed by calculating the theoretical convergence rate β from (5.15) for the approximate return maps (using the estimated T) shown in the table, which are substantially smaller than unity.

It is hoped that the condition of phase uniformity within regions can be relaxed in future work. For instance, by extending the calculations described

Image	*1*	*2*	*3*
λ_{lo}	0.10	0.10	0.10
λ_{hi}	0.08	0.06	0.04
w	0.05	0.05	0.05
σ	2.0	2.0	2.0
t_d	0.015	0.015	0.020
t_1 observed	1.969	1.691	1.711
t_2 observed	2.388	2.110	2.134
T observed	0.419	0.419	0.423
U_Δ predicted	0.8093	0.8434	0.9866
$U(t_1)$ observed	0.8096	0.8475	0.9860
$U(t_2)$ observed	0.8097	0.8454	0.9860
β	0.0451	0.0451	0.0450

Table 1: Comparing numerically observed and analytically predicted data relating to the long-term stability of a sub-threshold periodic solution.

in Bressloff & Coombes [4] and Chow [8] to the present model it may be possible to determine the linear stability of the long-term phase-locked state in each of the two regions separately. An estimate of the basin of attraction around this state in terms of the size of phase perturbations may then yield an estimate to the permissable heterogeneity in the image inputs which caused them (or in other sources of variation).

5.3 Connecting the transient and long-term dynamics

Following the suppression of neuron 2, $U_2(t)$ will increase once more as the inhibitory response decays, and the mechanism must prevent neuron 2 from firing again in order to make the transition to the phasic regime. It was noted in the numerical results that for low values of σ the succesful causing of a turning point in $U_2(t)$ may not be enough to prevent the excitatory forcing bringing the potential to threshold soon after. Thus it would be useful to derive a further condition on the parameters so that a turning point occurs and that $U_2(t)$ remains sub-threshold during the input burst. It may be possible to do this by extending the argument for the sub-threshold condition of the long-term solution to include the effects of the image input spike trains. For instance, under a worst case assumption on the excitatory inputs, an upper bound on the ISI of the *net* inhibitory input to the suppressed neuron for $t < t_{burst}$ can give estimated bounds on the parameters for $U_2(t)$ to remain sub-threshold until $t > t_{burst}$. Furthermore, these bounds become

less stringent as σ increases. (Chow performed a similar calculation for an IF network without shunting terms in Ref. [8].) For sufficiently strong coupling it was found from the simulations and estimation of the various quantities involved that most of the parameter regimes used here do fall within such a bound. We do not present the details here: a more careful analysis will be developed in future work.

6 Discussion

This paper has presented a robust mechanism for distinguishing simple gradients in a one-dimensional input represented by the ISIs of a set of spike bursts. The network 'sharpens' *significant* gradients in the input whilst 'cleaning up' small gradients (e.g. from noise) (see Figures 4, 5). Thus we can consider this as a simple model of feature detection. Certain analysis of the network is possible despite the complexities of the coding and additional biological features of the model. Accurate prediction of parameter regimes for successful detection would not be possible if the features problematic to analysis were stripped from the model. For instance, the inclusion of shunted inputs and absolute refractoriness is crucial to the robustness of the mechanism. Without these added characteristics the detection mechanism was found to occupy a tiny domain of parameter space and to be much less robust.

By using simulations to highlight relevant aspects of the dynamics of the full system, an analysis of the important aspects of the mechanism was possible by applying an ansatz and a similar reduction technique to those used by Bressloff & Coombes [4] to study other architectures. Their techniques have recently been generalised to cover strongly-connected networks of pulse-coupled neurons whose intrinsic dynamics can be described on $\mathbf{S}^1$ ([3]). In future work this generalisation to systems of discontinuous circle maps will be explored as a path to a more comprehensive understanding of the topological structure underlying models that retain several biologically realistic features (see also Refs. [12][5]).

The analytical treatment of the onset of oscillator death in Section 5.1 shows how the principal system parameters might be tuned to provide detection for a wide class of images, and analysis of the long-term state of oscillator suppression in Section 5.2 also indicates the dependence of its stability on these parameters. In particular the spike propagation delay t_d and coupling strength σ emerged as intuitive parameters determining the sensitivity of the network to contrasts, and to variations in the input in general. However, the mechanism also appears to depend on a balance between the values of all the other system parameters, although the detailed nature of this balance has not been investigated.

An intuitive argument in Section 5.3 linked the transient and long-term analyses together, which may account for the observed tendency for the

transient dynamics of oscillator suppression during the image input burst to quickly stabilise towards a long-term stable state of suppression in the phasic regime for a wide range of parameter choices. For instance, the simulations show that even if t_d is too large for detection with zero transient spikes to occur, then detection will typically ensue after one transient spike. For still higher values of t_d detection with two or more transient spikes is possible (see Figure 5). Thus the mechanism is more robust than the current analysis suggests, which for simplicity focused on the effect with zero transient spikes only. It was also observed that larger σ values ensured the transition to the phasic regime.

The occurrence of additional and unwanted oscillator deaths in simulation runs correlates to low values of t_d and small discrepancies between the phases within a region. In such a case the system is over-sensitive to drift in the group's firing times, so that it is possible for the arrival of some spikes to accidentally cause oscillator death. In practice, the drift in firing times may originate from several sources, both artificial and natural, e.g. noisy or 'blurred' contrasts in the image input data, natural heterogeneity in the intrinsic parameters of non-identical neurons, and the fact that neurons either side of the boundary are only receiving approximately half the input current per cycle because of their suppressed neighbour (these two neurons will therefore be inhibited less than the others in their respective groups, and will begin to lead them).

These over-sensitivities in the feature detector may be remedied by modelling biologically plausible forms of synaptic *adaptiveness*, either in terms of learning or by intrinsic dynamics associated with real synaptic responses. The connectivity in the detector chain itself could also be made more sophisticated. For instance, the nearest neighbour connections could be augmented with a distribution of local connections to other neurons in the chain to model a receptive field (RF). It is likely that an RF such as the classic symmetric 'mexican hat' function would perform local spatial averaging of image inputs for neurons far from an edge, whilst locally accentuating the image contrast near an edge, thus improving the efficiency of the network.

A Appendix

The exact analytical expression of $h(\cdot)$ was omitted from the main text for clarity, due to implementation issues concerning inter-neuronal 'spikes' in simulations using MATLAB's Simulink toolbox. Spikes were represented by square-wave impulses

$$F(t) = \begin{cases} 0, & t < t_{arr} \\ 50, & t_{arr} \leq t \leq t_{arr} + 0.02 \\ 0, & t > t_{arr} + 0.02 \end{cases} , \tag{A.1}$$

where t_{arr} is the arrival time of an incoming spike at a synapse. These signals were used to force a second order model of the synapse

$$\frac{1}{\alpha_1\alpha_2}\frac{d^2h(t)}{dt^2} + \left(\frac{\alpha_1+\alpha_2}{\alpha_1\alpha_2}\right)\frac{dh(t)}{dt} + h(t) = F(t), \quad h(0) = 0,\ t > 0, \quad \text{(A.2)}$$

where $\alpha_1 > \alpha_2$ is assumed. Thus the solution to this system gives the explicit form of $h(\cdot)$ used for numerical calculations:

$$h(t) = \begin{cases} 0 & t \leq 0 \\ 50 + 112.5e^{-130t} - 162.5e^{-90t} & 0 < t \leq 0.02 \\ 135.639e^{1.8-90t} - 104.144e^{2.6-130t} & t > 0.02 \end{cases}, \quad \text{(A.3)}$$

where $\alpha_1 = 130$ and $\alpha_2 = 90$. If (A.2) were unforced ($F \equiv 0$) and given unit initial condition its output would be the solution to the generalised 'difference of exponentials' representation of synaptic response,

$$h(t) = \frac{\alpha_1\alpha_2}{\alpha_2 - \alpha_1}\left(e^{-\alpha_1 t} - e^{-\alpha_2 t}\right)\Theta(t), \quad \text{(A.4)}$$

which reduces to the standard alpha function (2.7) in the limit $\alpha_1 \to \alpha_2 \to \alpha$. However, the form of $h(\cdot)$ used here (A.3) resembles that of (A.4) spread over a longer time (so having a slower increasing slope), and both satisfy the conditions (2.6) used in the analysis.

Acknowledgements

The author would like to thank Alan Champneys and Steve Coombes for helpful discussions and assistance in proof reading the manuscript. This work was supported by the EPSRC.

References

[1] Abbott, L.F., Realistic synaptic inputs for model neural networks, *Network*, 2:245-258, 1991.

[2] Barlow, H.B. and Mollon, J.D., eds., *The Senses*, Cambridge University Press, Cambridge, 1989.

[3] Bressloff, P.C., Phase-locking instabilities in networks of synaptically coupled neural oscillators, *Preprint*, 1999.

[4] Bressloff, P.C. and Coombes, S., Dynamics of strongly-coupled spiking neurons, *Neural Computation*, 12:91-129, 2000.

[5] Bressloff, P.C. and Stark, J., Neuronal dynamics based on discontinuous circle maps, *Phys. Lett. A*, 150(3):187-195, 1990.

[6] Bressloff, P.C. and Taylor, J.G., Discrete time leaky integrator network with synaptic noise, *Neural Networks*, 4:789-801, 1991.

[7] Char, B. W., et al., *Maple V language reference manual*, Springer, Berlin, 1995.

[8] Chow, C.C., Phase-locking in weakly heterogeneous neuronal networks, *Physica D*, 118:343-370, 1998.

[9] Coombes, S. and Lord, G.J., Desynchronisation of pulse-coupled integrate-and-fire neurons, *Phys. Rev. E*, 55(3):2104-2107, 1996.

[10] Eckhorn, R., Stimulus-evoked synchronizations in the visual cortex: linking of local features into global figures?, In *Neural Cooperativity*, Krüger, J., ed., Springer Series in Brain Dynamics, Springer-Verlag, 1989.

[11] Ermentrout, G.B., Type I membranes, phase resetting curves, and synchrony, *Neural Computation*, 8:979-1001, 1996.

[12] Ernst, U., Pawelzik, K. and Giesel, T., Synchronization induced by temporal delays in pulse-coupled oscillators, *Phys. Rev. Lett.*, 74(9):1570-1573, 1995.

[13] Gerstner, W., Spiking Neurons. Chapter 1 of *Pulsed Neural Networks*, Maas, W. and Bishop, C.M., eds., MIT Press, 1998.

[14] Gerstner, W., Kreiter, A.K., Markram, H. and Herz, A.V.M., Neural codes: Firing rates and beyond, *Proc. Natl. Acad. Sci. USA*, 94:12740-12741, 1997.

[15] Gray, C.M., König, P., Engel, A.K. and Singer, W., Oscillatory responses in cat visual cortex exhibit inter-columnar synchronization which reflects global stimulus properties, *Nature*, 338:334-337, 1989.

[16] Hopfield, J.J., Pattern recognition computation using action potential timing for stimulus representation, *Nature*, 376:33-36, 1995.

[17] Horn, D. and Opher, I., Collective excitation phenomena and their applications. Chapter 11 of *Pulsed Neural Networks*, Maas, W. and Bishop, C.M., eds., MIT Press, 1998.

[18] Jack, J., Noble, D. and Tsien, R., *Electric Current Flow in Excitable Cells*, Clarendon Press, Oxford, 1975.

[19] Keener, J., Hoppensteadt, F.C. and Rinzel, J., Integrate-and-fire models of nerve membrane response to oscillatory input, *SIAM J. Appl. Math.*, 41(3):503-517, 1981.

[20] von der Malsburg, C. and Buhman, J., Sensory segmentation with coupled neural oscillators, *Biol. Cybern.*, 67:233-242, 1992.

[21] Markram, H. and Tsodyks, M., Redistribution of spike timing in neocortical neurons, *Science*, 268:1503-1506, 1996.

[22] Neuenschwander, S. and Singer, W., Long-range synchronization of oscillatory light responses in the cat retina and lateral geniculate nucleus, *Nature*, 379:728-733, 1996.

[23] Nischwitz, A. and Glünder, H., Local lateral inhibition: a key to spike synchronization?, *Biol. Cybern.*, 73:389-400, 1995.

[24] Rieke, F., Warland, D., de Ruyter van Steveninck, R.R. and Bialek, K., *Spikes: Exploring the neural code*, MIT Press, Cambridge, MA, 1997.

[25] Shadlen, M.N. and Newsome, W.T., The variable discharge of cortical neurons: Implications for connectivity, computation, and information coding, *The Journal of Neuroscience*, 18(10):3870-3896, 1998.

[26] Shampine, L.F. and Reichelt, M.W., The MATLAB ODE Suite, *SIAM Journal on Scientific Computing*, Volume 18, 1997.

[27] Shepherd, G.M., *Neurobiology*, Second Edition, Oxford University Press, Oxford, 1988.

[28] van Vreeswijk, C., Abbott, L.F. and Ermentrout, G.B., When inhibition not excitation synchronizes neural firing, *J. Comp. Neurosci.*, 1:313-321, 1994.

[29] Wang, D.L. and Terman, D., Image segmentation based on oscillatory correlation, *Neural Computation*, 9:805-836, 1997.

[30] White, J.A., Chow, C.C., Ritt, J., Soto-Treviño, C. and Kopell, N., Synchronization and oscillatory dynamics in heterogeneous, mutually inhibited neurons, *J. Comp. Neurosci.*, 5:5-16, 1998.